

Anomalous thermal conductivity in 2D silica nanocages of immobilizing noble gas atom

Yang Wang,¹ Zhibin Gao,^{1,†} Xiaoying Wang,¹ Jinping Sun,² Minxuan Feng,¹ Yuzhou Hao,¹ Xuejie Li,¹ Yinchang Zhao,^{3,†} and Xiangdong Ding¹

¹*State Key Laboratory for Mechanical Behavior of Materials, School of Materials Science and Engineering, Xi'an Jiaotong University, Xi'an 710049, China*

²*School of Materials Science and Engineering, Harbin Institute of Technology at Weihai, 2 West Wenhua Road, Weihai 264209, China*

³*Department of Physics, Yantai University, Yantai 264005, China*

Noble gas atoms, such as Kr and Xe are byproducts of nuclear fission in nuclear plants. How to trap and confine these volatile even radioactive gases is particularly challenging. Recent studies have shown that they can be trapped in nanocages of ultrathin silica. Here we exhibit with self-consistent phonon (SCP) theory and four-phonon (4ph) scattering where the adsorption of noble gases results in an anomalous increase in lattice thermal conductivity (κ_L), while the presence of Cu atoms doping leads to a reduction in κ_L . We trace this behavior in host-guest 2D silica to an interplay of tensile strain, rattling phonon modes, and redistribution of electrons. We also find that 4ph scatterings play indispensable roles in κ_L of 2D silica. Our work illustrates the microscopic heat transfer mechanism in 2D silica nanocages with the immobilization of noble gas atoms and inspires further exploring materials with the kagome and glasslike κ_L .

Silicon dioxide (silica), one of the most abundant materials in the earth's crust, constitutes a fundamental component of glass, sand, and the majority of minerals. With the advancement of nanomaterial fabrication technology, single-crystal two-dimensional (2D) silica films, using chemical vapor deposition (CVD), can be successfully grown on metal Mo(112) [1], Ru(0001) [2], and even graphene substrate [3, 4]. This thinnest insulating material exhibits distinctive features [5], and are also useful in confined chemical reaction [6], subatomic species transport [7], and radioactive gas separation [8]. Moreover, atomically smooth 2D silica can be mechanically exfoliated and transferred to the support at millimeter scale [9]. This property renders it suitable for catalysis and the isolation of graphene from metal substrates, facilitating the creation of vertically transferable heterostructures [10–12] and ultrathin gate oxides in field effect transistors [13].

Radioactive isotopes of noble gases Krypton (Kr) and Xenon (Xe) are a byproduct of nuclear fission in nuclear plants [14–16]. Compared to electrostatic trapping, the only approach to trap noble gas at room temperature is the ion implantation [17, 18], forming a 2D silicate-noble gas clathrate compounds [8, 15, 16].

Introducing guest atoms in host-guest systems like clathrate can effectively reduce their κ_L . Concurrently, the rattling modes derived from guest atoms significantly enhance the scattering phase space and reduce phonon relaxation time (τ), resulting in a decrease in κ_L [19, 20]. Therefore, the application of 2D silica nanocage for capturing fission gases may potentially further amplify temperature gradients within nuclear fuels, compromising safety.

In the recently scrutinized lead-phosphate crystal $\text{Pb}_{10}(\text{PO}_4)_6\text{O}$ (LK-99), which underscores the pivotal

role played by Cu atoms in the modulation of electronic properties [21]. Noble gas atoms possess saturated electron structures, and doping noble gas atoms can yield more idealized models. Hence, contrasting host-guest systems doped with Cu atoms and noble gas atoms allow for separate consideration of the mechanism by which electron density distribution and phonon-phonon scatterings [22].

In this study, we investigated the microscopic heat transfer mechanism in the 2D silica nanocages. The results indicate contrasting effects of adsorbed noble gas and Cu atoms on the κ_L of 2D silica. On one hand, the adsorption of the Kr atom induces tensile strain in the host system, decreasing phonon scattering probabilities and resulting in an increase in κ_L . On the other hand, Cu atom doping confines the electronic distribution of the nanocage and suppresses strain in the host system. Moreover, substantial flat bands emerge in the low-frequency acoustic phonon branch, enhancing phonon-phonon scattering through rattling modes, leading to a reduction in κ_L .

DFT calculations were performed using the Vienna ab initio simulation package (VASP) [23]. The interaction between valence electrons and ions is realized by the functional of Perdew-Burke-Ernzerhof (PBE) [24] and the generalized gradient approximation (GGA) with projector augmented wave (PAW) [25]. The format of the second-order interatomic force constants (2nd-IFCs) file from the AlamoD [26] was transformed into the Sheng-BTE interface [27]. For three-phonon (3ph) and 4ph scatterings, we used a uniform $40 \times 40 \times 1$ and $7 \times 7 \times 1$ q-mesh grids [28]. More details are in the Supplementary Material.

Top and side views of 2D silica with $P6/mmm$ symmetry are depicted in Fig. 1 (a-b). The primitive cell

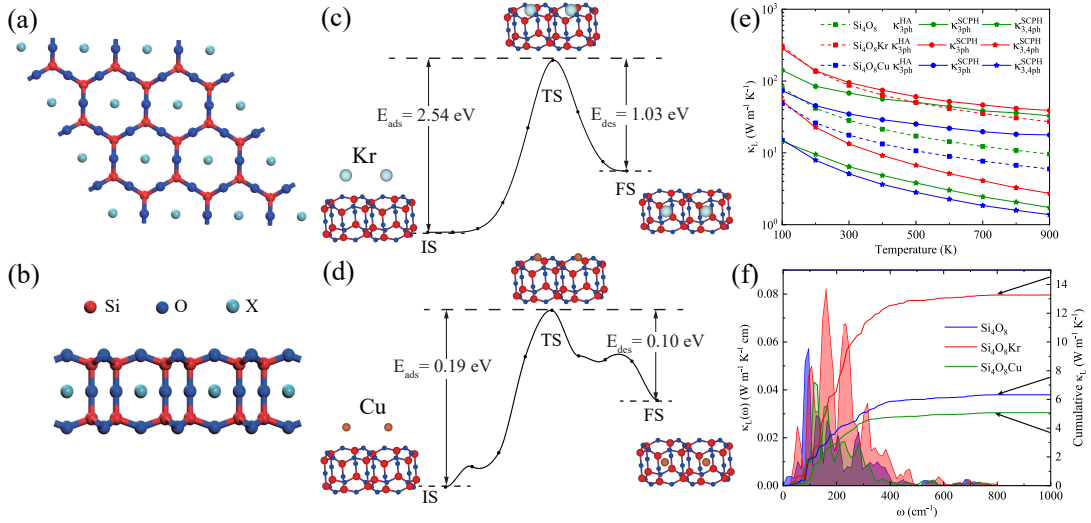


FIG. 1. (a)-(b) The top and side views of the 2D-Si₄O₈ crystal structure with doped X atoms (X=Ar, Kr, Xe, Cu). The red, blue, and cyan colors represent silicon (Si), oxygen (O), and doped atoms X. (c)-(d) The minimum energy path for doping Kr and Cu atoms. (e) κ_{3ph}^{HA} , κ_{3ph}^{SCPH} and $\kappa_{3,4ph}^{SCPH}$ as a function of temperature. Si₄O₈, Si₄O₈Kr, and Si₄O₈Cu represent undoped, Kr-doped, and Cu-doped silica. (f) The κ_L spectrum of the frequency distribution in the shaded areas and cumulative κ_L as a function of frequency in solid lines.

consists of 4 silicon atoms and 8 oxygen atoms with an optimized lattice constant of $a = b = 5.312$ Å.

Due to the minimization of structure energy, the doping atom precisely stays at the center of the nanocage to keep stability. We computed the phonon spectra for a series of atom dopings, as shown in Fig. S1-S2. We find that the large electronegativity difference between the guest atoms and the host lattice could lead to structural instability since excess dopant electrons will cause a collapse of the nanocage. Furthermore, noble gas atoms possess a saturated electron orbit and can also be stable on the framework electron structure of 2D-Si₄O₈ [29].

The dynamic stability of structures with phonon spectrum is further assessed. It is worth noting that the adsorbed noble gas atoms results are stable isotopes in the calculation. The minimum energy path for doping atoms are calculated using climbing image nudged elastic band (CI-NEB) calculations [30]. The activation energies for the adsorption and desorption of Ar, Kr, Xe, and Cu doping atoms within the nanocage are shown in Fig. 1 (c)-(d) and Fig. S3. This indicates that adsorbed atoms can be captured and released into the nanocage with proper activation energies of E_{ads} and E_{des} . Due to the similar properties exhibited by noble gases, in the following, we examine variations in κ_L using Kr and Cu atoms as examples.

κ_{3ph}^{HA} , κ_{3ph}^{SCPH} , $\kappa_{3,4ph}^{SCPH}$ of Si₄O₈, Si₄O₈Kr, and Si₄O₈Cu versus temperature are showed in Fig. 1 (e). This result indicates an anomalous increase in κ_L after Kr doping and a decrease in κ_L after Cu doping. The influence of renormalization and 4ph scattering on κ_L is elucidated through the ratios in the Fig. 2 (c). SCPH is the ab-

breivation of self-consistent phonon with temperature-dependent phonon frequencies [31, 32]. $\kappa_{3ph}^{SCPH}/\kappa_{3ph}^{HA}$ reflects the impact of phonon frequency (ω) shifts due to temperature-dependent phonons. $\kappa_{3,4ph}^{SCPH}/\kappa_{3ph}^{HA}$ indicates the complete effect of 4th-order anharmonicity and $\kappa_{3,4ph}^{SCPH}/\kappa_{3,4ph}^{SCPH}$ reflects the additional influence of 4ph scattering on top of the 3ph process. In the Si₄O₈, Si₄O₈Kr and Si₄O₈Cu, the values of $\kappa_{3,4ph}^{SCPH}/\kappa_{3ph}^{SCPH}$ are 0.094, 0.141, and 0.147, respectively. This indicates that 4ph scattering significantly increases the phonon scattering. Moreover, all three materials exhibit strong phonon frequency shift effects, as evidenced by the relatively large values of $\kappa_{3ph}^{SCPH}/\kappa_{3ph}^{HA}$. Generally, 4ph scattering decreases κ_L while the SCPH increases κ_L . In a practical situation, both 4ph scattering and phonon frequency shift compete in determining the final κ_L [31]. The values of $\kappa_{3,4ph}^{SCPH}/\kappa_{3ph}^{HA}$ for Si₄O₈, Si₄O₈Kr, and Si₄O₈Cu are 0.226, 0.153, and 0.289, indicating that 4ph scattering plays a more substantial role than the normalized phonon frequency shift in all three materials.

The thermal conductivity spectrum $\kappa_L(\omega)$ and cumulative κ_L at 300 K are shown in Fig. 1 (f). Low-frequency acoustic phonons contribute significantly to κ_L . To elucidate the abnormal heat transport mechanism of doping, we obtain the phonon dispersions and phonon density of states (PDOS), as shown in Fig. 2 (a). Apparently, none of the materials exhibit imaginary frequencies in the harmonic approximation (HA), indicating the dynamic stability of these structures. The PDOS reveals that Si₄O₈ features a flat phonon mode in the mid-frequency range ($\omega = 120$ -150 cm⁻¹). However, doping with the Kr atom eliminates the low-frequency flat mode. Cu atom doping

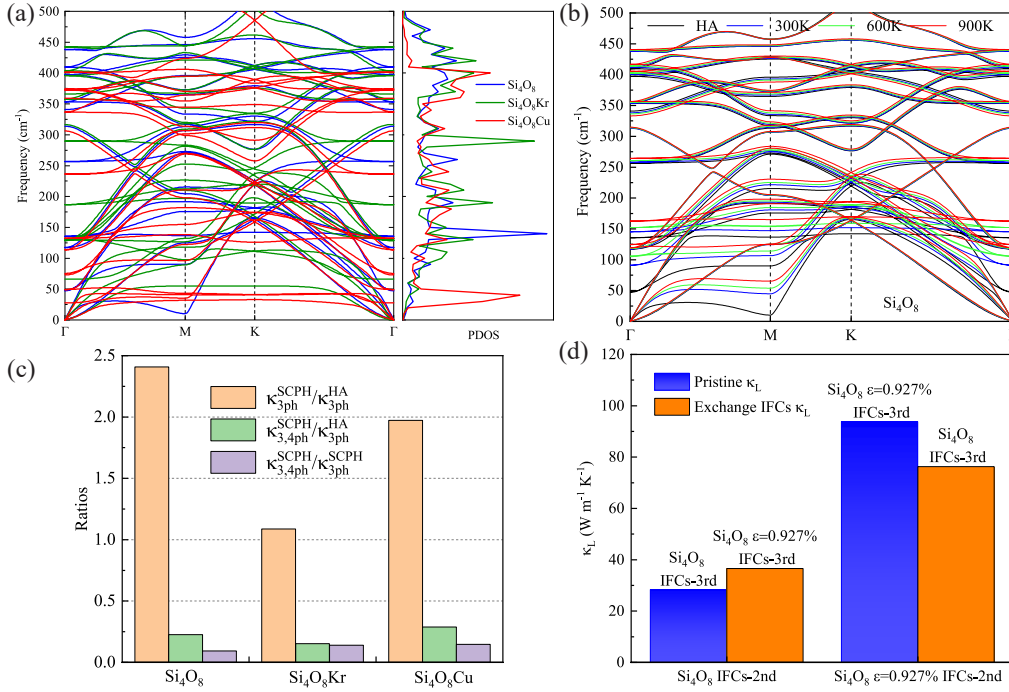


FIG. 2. (a) Phonon dispersions and phonon density of states (PDOS). (b) The normalized phonon dispersion of Si₄O₈ at different temperatures. (c) The ratio of $\kappa_{3ph}^{SCPH}/\kappa_{3ph}^{HA}$, $\kappa_{3,4ph}^{SCPH}/\kappa_{3ph}^{HA}$, $\kappa_{3,4ph}^{SCPH}/\kappa_{3ph}^{SCPH}$ at 300 K. (d) κ_L of 2D silica without strain and $\epsilon = 0.927\%$ strain calculated by the exchange IFCs at 300 K. The abscissa is the 2nd-IFCs and the column is marked with the third-order interatomic force constants (3rd-IFCs) for κ_L .

introduces a rattling mode, particularly leading to significant flattening of the low-frequency phonon branch ($\omega = 20\text{--}50\text{ cm}^{-1}$). These rattling modes increase the phonon-phonon scattering [33].

The result indicates that the flat mode is primarily influenced by the vibrations of the filling atoms within the nanocages, and doping of the Cu atom plays an important role in the rattling modes of the atomic vibrations. In clathrate structures, the extremely low κ_L due to doping arises from the absence of avoided dispersion crossings of filling modes, significantly enhancing scattering channels [20, 34–36].

Comparing the temperature-dependent phonon spectrum of Si₄O₈ at 0 K, 300 K, and 900 K, these three materials exhibit dynamical support stability as shown in Fig. 2 (b) and Fig. S4. There is an obvious phonon hardening phenomenon.

Firstly, we explore the reason for the decrease in κ_L of Si₄O₈Cu. Fig. S5 (a) shows the calculated heat capacity (C_V) of Si₄O₈, Si₄O₈Kr, and Si₄O₈Cu as a function of temperature. It can be seen that the C_V of Si₄O₈Cu is the highest, which is in contrast to the observed reduction in κ_L of Si₄O₈Cu. The change of phonon group velocities is small due to the doping, as shown in Fig. S5 (b).

Next, it is further considered that τ plays an important role in reducing κ_L of Si₄O₈Cu. We have plotted the curve of τ as a function of phonon frequency, represented by $1/\tau = \omega/2\pi$. Once the single relaxation time

exceeds the curve of $1/\tau = \omega/2\pi$, indicating that the τ is shorter than one vibrational period, the phonon quasi-particle picture is no longer valid [31]. As shown in Fig. 3 (a)-(c), the majority of 3ph and 4ph scattering events are distributed below the $1/\tau = \omega/2\pi$ curve, confirming the validity of the BTE solution in this study [27, 37, 38].

We interpret the difference in κ_L among Si₄O₈, Si₄O₈Kr, and Si₄O₈Cu based on their phonon scattering rates (SRs), as shown in Fig. 3 (a)-(c) and Fig. S6. In Si₄O₈Cu, the scattering rates are nearly an order of magnitude higher than those in Si₄O₈ at most frequencies. Cu doping induces significantly higher scattering rates, leading to a reduction in κ_L [33]. To further explore the potential mechanism behind the strong 4ph scattering, we analyzed the 3ph and 4ph scattering phase spaces of Si₄O₈, Si₄O₈Kr and Si₄O₈Cu at 300 K. The results indicate that the scattering phase space of Si₄O₈Kr increases upon doping with the Kr atom, while the Cu atom doping introduces rattling modes, causing a reduction in flat band frequencies. This significantly enhances the scattering channels and increases the scattering probability, as shown in Fig. 3 (e)-(f) and Fig. S7.

Interestingly, there is an anomalous increase in κ_L upon doping with the Kr atom. Despite Si₄O₈ being an ultrahard material, a lattice strain of 0.927% was observed in Si₄O₈Kr, resulting in a κ_L of 87.306 W m⁻¹ K⁻¹ at 300 K, as shown in Table 1. Subsequently, we calculated the κ_L of Si₄O₈ when subjected to a 0.927

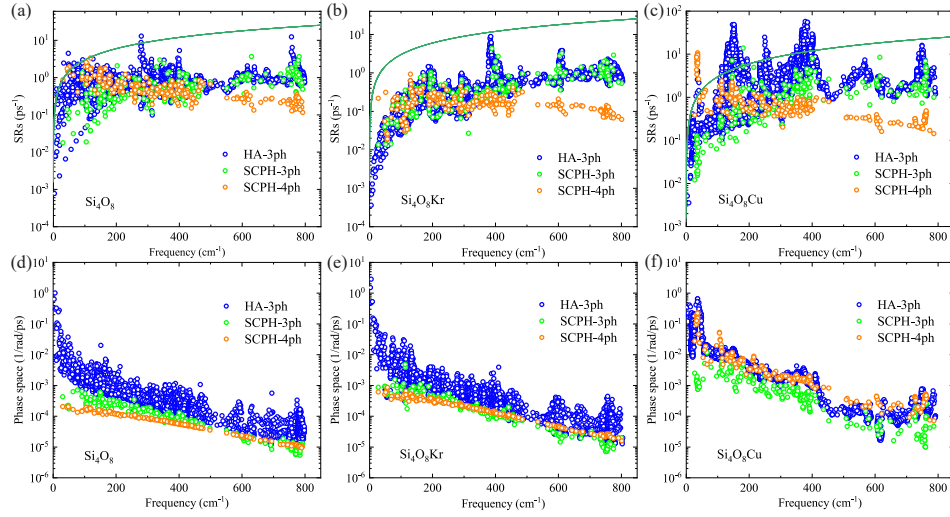


FIG. 3. (a)–(c) Scattering ratios (SRs) and (d)–(f) weighted phase space as a function of frequency of Si_4O_8 , $\text{Si}_4\text{O}_8\text{Kr}$ and $\text{Si}_4\text{O}_8\text{Cu}$ at 300 K. The blue, green, and orange colors represent 3ph scattering affected by the harmonic approximation (HA-3ph), 3ph scattering affected by SCPH (SCPH-3ph), and 4ph scattering affected by SCPH (SCPH-4ph). The solid green lines in (a)–(c) show that the scattering rate is equal to the phonon frequency ($1/\tau = \omega/2\pi$).

% strain, resulting in κ_L of $93.788 \text{ W m}^{-1} \text{ K}^{-1}$ at 300 K, as displayed in Table 1. We observed that the κ_L of strained Si_4O_8 is higher than that of Si_4O_8 doped with the Kr atom. Therefore, the enhanced κ_L in $\text{Si}_4\text{O}_8\text{Kr}$ primarily arises from the framework strain induced by the doping, rather than the rattling mode. This framework strain leads to an upward shift in the phonon spectrum, especially for the acoustic and low-frequency optical branches, as shown in Fig. 2 (a). Concurrently, Kr doping contributes to the reduction in κ_L .

Next, we compare the impact of harmonic and anharmonic contributions by exchanging the IFCs. Subsequently, the impact of lattice strain induced by exchanging harmonic and anharmonic IFCs on κ_L is examined. As shown in Fig. 2 (d), the horizontal axis represents the input 2nd-IFCs, and annotations at the top of the bars indicate the input 3rd-IFCs, facilitating the computation of κ_{3ph}^{HA} . Columns 1 and 4 share the same 3rd-IFCs, while their 2nd-IFCs differ. Exchanging force constants results in an increased κ_L , approaching κ_L of Column 3 (Si_4O_8 $\varepsilon = 0.927\%$). Therefore, under the influence of strain, harmonic effects emerge as the primary contributing factor to the increase in κ_L upon doping of 2D silica. Simultaneously, under the influence of strain induced by doping, both scattering rates and phase space decrease, corresponding to the observed increase in κ_L , as shown in Fig. S8-S9. The tensile strain effect on the κ_L of 2D silica are shown in Fig. S10.

By comparing the relative atomic mass of doping atoms in Table 1, it is evident that the doping atom X (X=Ar, Kr, and Xe) does not interact significantly with the host framework. The larger the mass of the doping atom, the greater the strain it induces. This phe-

nomenon aligns with the behavior observed after applying the strain on the 2D silica [39]. For instance, when the Cu atom is doped, it induces a framework strain of only 0.007 %, significantly smaller than the strain produced after doping with the Ar atom, which amounts to 0.584 %. Despite copper (Cu) having a greater relative atomic mass than argon (Ar), the strain of framework induced by Cu is even smaller than that induced by Ar. Therefore, it becomes necessary to consider the electronic interaction and distribution between the doped Cu atom and the host framework.

Thus, we conduct differential charge density calculations of $\text{Si}_4\text{O}_8\text{Kr}$ and $\text{Si}_4\text{O}_8\text{Cu}$ to investigate the change in electronic distribution. The regions with significant variations in the framework are attributed to the doping atom. On the one hand, since the Kr atom is in a chemical full-shell state and doping Kr will redistribute and squeeze the electron distribution of the framework, leading to the electrons moving to both sides in Fig. 4 (a). On the other hand, the Cu atoms have a strong attraction with the host framework, gathering the electrons toward the center in Fig. 4 (b). Fig. 4 (c)–(d) display the electron localization function (ELF). In $\text{Si}_4\text{O}_8\text{Kr}$, the interaction between Kr atoms and the framework is relatively weak, leading to high electronic localization near the Kr atom. After the doping of Cu atoms, stronger interaction occurs between Cu atoms and the framework, resulting in smaller localization near Cu atoms. Combined with Bader charge analysis, it is shown that the doping of Cu and Kr atoms does not lead to the formation of chemical bonds with the host framework [40].

Subsequently, partial electron density analysis is performed on the atomic character bands of Cu and Kr, as

TABLE I. The Influence of doped atomic mass on the change of lattice constant (a) and strain effect of Si_4O_8 and $\text{Si}_4\text{O}_8\text{X}$ (X = Cu, Ar, Kr, and Xe).

	Mass of X (u)	a (Å)	Strain ε (%)	κ_L ($\text{W m}^{-1} \text{K}^{-1}$)	$\kappa_L / \kappa_L (\text{Si}_4\text{O}_8)$
Si_4O_8	0	5.312	0	28.289	1
Si_4O_8	0	5.361	0.927	93.788	3.315
$\text{Si}_4\text{O}_8\text{Cu}$	63.55	5.312	0.007	17.648	0.624
$\text{Si}_4\text{O}_8\text{Ar}$	39.95	5.343	0.584	80.821	2.857
$\text{Si}_4\text{O}_8\text{Kr}$	83.80	5.361	0.927	87.312	3.112
$\text{Si}_4\text{O}_8\text{Xe}$	131.29	5.397	1.600	121.405	4.291

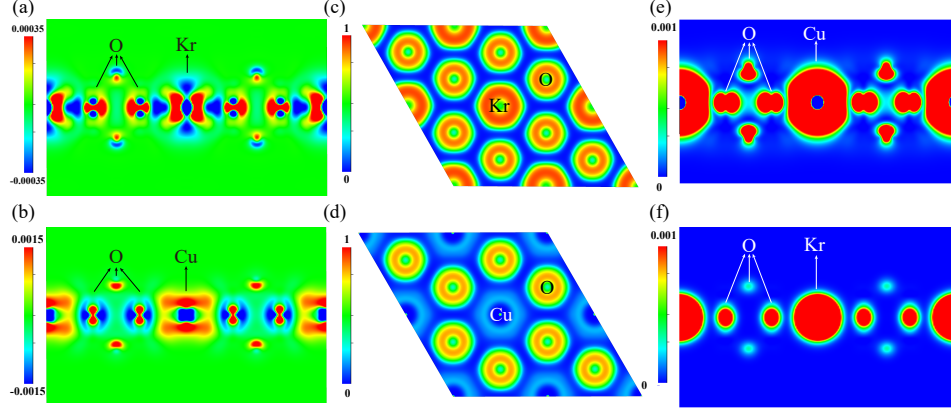


FIG. 4. Effect of doping Kr and Cu atoms on the electron density of nanocages. (a)-(b) 2D projection of the differential electron density function on the (110) plane, the selection charge density ranges of $\text{Si}_4\text{O}_8\text{Kr}$ and $\text{Si}_4\text{O}_8\text{Cu}$ are ± 0.00035 and $\pm 0.0015 e \cdot \text{bohr}^{-3}$ respectively. (c)-(d) 2D projection of the electron local function (ELF) on the (001) plane (e)-(f) 2D projection of the partial electron density function of Kr and Cu atoms in Si_4O_8 . Selected partial charge densities ranging from 0 (blue) to $0.001 e \cdot \text{bohr}^{-3}$ (red).

shown in Figure 4 (e)-(f). By comparing the results of $\text{Si}_4\text{O}_8\text{Kr}$ and $\text{Si}_4\text{O}_8\text{Cu}$, it is found that a noticeable enhancement in the interaction between Cu guest atoms and the host nanocages, indicating a certain level of electronic interaction. However, it should be noted that the doping atoms did not form chemical bonds with the host framework, thus inhibiting large strain on the framework. In the case of the noble gas atom Kr, the interaction with the host cage was significantly weaker, primarily due to the absence of electronic interaction between the guest atoms and the host nanocage electrons.

In summary, we have studied the effect of adsorbed noble gas and copper atoms on κ_L of 2D silica nanocages based on temperature-dependent phonons through self-consistent phonon theory and fourth-order multiphonon scattering. The adsorption of noble gases results in an anomalous increase in κ_L , while the presence of Cu atoms leads to a reduction in κ_L . Adsorption of noble gas atoms on 2D silica results in tensile lattice strain within the nanocages, reducing phonon scattering rates and consequently leading to an increase in κ_L . In contrast to the weak interaction between noble gas atoms and the nanocages, Cu atom doping confines the distribution of electronic states without inducing significant

strain in the nanocage, through its interaction with the nanocage electrons. The introduction of Cu atoms induces significant broadening and frequency shifts in the low-frequency phonon branches of the system, leading to the creation of large flat bands. This alteration, coupled with the enhancement of phonon scattering probability through rattling modes, results in a reduction of κ_L .

Our results illustrate the microscopic heat transfer mechanism of adsorbed atoms in 2D silica nanocages, emphasizing the significant roles of lattice distortion and changes in electron density distribution in the κ_L . We also show the four-phonon scatterings play an indispensable role in the computation of κ_L of 2D silica. Our study might inspire further theoretical and experimental investigations exploring materials with the kagome and glasslike κ_L [31, 41, 42].

See the Supplementary Material for the phonon spectrum, the minimum energy path for doped Ar and Xe atoms, the renormalized phonon dispersion at different temperatures, heat capacity as a function of temperature, phonon group velocity, Grüneisen parameter, phonon scattering rates, phonon phase space and κ_L of 2D silica with applied tensile strain.

The authors acknowledge the support from the

National Natural Science Foundation of China (No.12104356 and No.52250191) and the Key Research and Development Program of the Ministry of Science and Technology (No.2023YFB4604100). Z.G. acknowledges the support of China Postdoctoral Science Foundation (No. 2022M712552), the Opening Project of Shanghai Key Laboratory of Special Artificial Microstructure Materials and Technology (No.Ammt2022B-1), and the Fundamental Research Funds for the Central Universities. We thank Prof. Mengyang Li for helping with the discussions.

AUTHOR DECLARATIONS

Conflict of Interest

The authors have no conflicts to disclose.

DATA AVAILABILITY

The data that support the findings of this study are available from the corresponding authors upon reasonable request.

[†] Authors to whom correspondence should be addressed: zhubin.gao@xjtu.edu.cn, and y.zhao@ytu.edu.cn

- [1] J. Weissenrieder, S. Kaya, J.-L. Lu, H.-J. Gao, S. Shaikhutdinov, H.-J. Freund, M. Sierka, T. K. Todorova, and J. Sauer, *Phys. Rev. Lett.* **95**, 076103 (2005).
- [2] D. Löffler, J. J. Uhlrich, M. Baron, B. Yang, X. Yu, L. Lichtenstein, L. Heinke, C. Büchner, M. Heyde, S. Shaikhutdinov, H.-J. Freund, R. Włodarczyk, M. Sierka, and J. Sauer, *Phys. Rev. Lett.* **105**, 146104 (2010).
- [3] P. Y. Huang, S. Kurasch, A. Srivastava, V. Skakalova, J. Kotakoski, A. V. Krashennnikov, R. Hovden, Q. Mao, J. C. Meyer, J. Smet, D. A. Muller, and U. Kaiser, *Nano Lett.* **12**, 1081 (2012).
- [4] P. Y. Huang, S. Kurasch, J. S. Alden, A. Shekhawat, A. A. Alemi, P. L. McEuen, J. P. Sethna, U. Kaiser, and D. A. Muller, *Science* **342**, 224 (2013).
- [5] Z. Gao, X. Dong, N. Li, and J. Ren, *Nano Lett.* **17**, 772 (2017).
- [6] M. J. Prieto, H. W. Klemm, F. Xiong, D. M. Gottlob, D. Menzel, T. Schmidt, and H.-J. Freund, *Angew. Chem. Int. Ed.* **57**, 8749 (2018).
- [7] P. R. Kidambi, P. Chaturvedi, and N. K. Moehring, *Science* **374**, eabd7687 (2021).
- [8] Y. Xu, M. Dorneles de Mello, C. Zhou, S. Sharma, B. Karagoz, A. R. Head, Z. Darbari, I. Waluyo, A. Hunt, D. J. Stacchiola, S. Manzi, A. M. Boscoboinik, V. D. Pereyra, and J. A. Boscoboinik, *Small* **17**, 2103661 (2021).
- [9] C. Büchner, Z.-J. Wang, K. M. Burson, M.-G. Willinger, M. Heyde, R. Schlögl, and H.-J. Freund, *ACS Nano* **10**, 7982 (2016).
- [10] M. A. Islam, J. H. Kim, A. Schropp, H. Kalita, N. Choudhary, D. Weitzman, S. I. Khondaker, K. H. Oh, T. Roy, H.-S. Chung, and Y. Jung, *Nano Lett.* **17**, 6157 (2017).
- [11] J. Hofrichter, B. N. Szafrank, M. Otto, T. J. Echtermeyer, M. Baus, A. Majerus, V. Geringer, M. Ramsteiner, and H. Kurz, *Nano Lett.* **10**, 36 (2010).
- [12] Q. Liu, Y. Gong, T. Wang, W.-L. Chan, and J. Wu, *Carbon* **96**, 203 (2016).
- [13] D. A. Muller, T. Sorsch, S. Moccio, F. Baumann, K. Evans-Lutterodt, and G. Timp, *Nature* **399**, 758 (1999).
- [14] S. Kawai, A. S. Foster, T. Björkman, S. Nowakowska, J. Björk, F. F. Canova, L. H. Gade, T. A. Jung, and E. Meyer, *Nat. Commun.* **7**, 11559 (2016).
- [15] J.-Q. Zhong, M. Wang, N. Akter, J. D. Kestell, A. M. Boscoboinik, T. Kim, D. J. Stacchiola, D. Lu, and J. A. Boscoboinik, *Nat. Commun.* **8**, 16118 (2017).
- [16] J.-Q. Zhong, M. Wang, N. Akter, J. D. Kestell, T. Niu, A. M. Boscoboinik, T. Kim, D. J. Stacchiola, Q. Wu, D. Lu, and J. A. Boscoboinik, *Adv. Funct. Mater.* **29**, 1806583 (2019).
- [17] H. Dil, J. Lobo-Checa, R. Laskowski, P. Blaha, S. Berner, J. Osterwalder, and T. Greber, *Science* **319**, 1824 (2008).
- [18] H. Cun, M. Iannuzzi, A. Hemmi, S. Roth, J. Osterwalder, and T. Greber, *Nano Lett.* **13**, 2098 (2013).
- [19] Z. Zhang, S. Hu, T. Nakayama, J. Chen, and B. Li, *Carbon* **139**, 289 (2018).
- [20] W. Li and N. Mingo, *Phys. Rev. B* **91**, 144304 (2015).
- [21] J. Lai, J. Li, P. Liu, Y. Sun, and X.-Q. Chen, *J. Mater. Sci. Technol.* **171**, 66 (2024).
- [22] J. Tang and J. M. Skelton, *J. Phys.: Condens. Matter* **33**, 164002 (2021).
- [23] G. Kresse and J. Furthmüller, *Phys. Rev. B* **54**, 11169 (1996).
- [24] J. P. Perdew, K. Burke, and M. Ernzerhof, *Phys. Rev. Lett.* **77**, 3865 (1996).
- [25] G. Kresse and D. Joubert, *Phys. Rev. B* **59**, 1758 (1999).
- [26] T. Tadano and S. Tsuneyuki, *Phys. Rev. B* **92**, 054301 (2015).
- [27] Y. Zhao, S. Zeng, G. Li, C. Lian, Z. Dai, S. Meng, and J. Ni, *Phys. Rev. B* **104**, 224304 (2021).
- [28] Z. Han, X. Yang, W. Li, T. Feng, and X. Ruan, *Comput. Phys. Commun.* **270**, 108179 (2022).
- [29] B. Duan, J. Yang, J. R. Salvador, Y. He, B. Zhao, S. Wang, P. Wei, F. S. Ohuchi, W. Zhang, R. P. Hermann, O. Gourdon, S. X. Mao, Y. Cheng, C. Wang, J. Liu, P. Zhai, X. Tang, Q. Zhang, and J. Yang, *Energy Environ. Sci.* **9**, 2090 (2016).
- [30] G. Henkelman, B. P. Uberuaga, and H. Jónsson, *J. Chem. Phys.* **113**, 9901 (2000).
- [31] X. Wang, Z. Gao, G. Zhu, J. Ren, L. Hu, J. Sun, X. Ding, Y. Xia, and B. Li, *Phys. Rev. B* **107**, 214308 (2023).
- [32] Y. Xia, V. I. Hegde, K. Pal, X. Hua, D. Gaines, S. Patel, J. He, M. Aykol, and C. Wolverton, *Phys. Rev. X* **10**, 041029 (2020).
- [33] T. Tadano, Y. Gohda, and S. Tsuneyuki, *Phys. Rev. Lett.* **114**, 095501 (2015).
- [34] J. Tse, D. Klug, J. Zhao, W. Sturhahn, E. Alp, J. Baumert, C. Gutt, M. Johnson, and W. Press, *Nat. Mater.* **4**, 917 (2005).
- [35] A. Prokofiev, A. Sidorenko, K. Hradil, M. Ikeda, R. Svagera, M. Waas, H. Winkler, K. Neumaier, and S. Paschen, *Nat. Mater.* **12**, 1096–1101 (2013).
- [36] M. Christensen, A. B. Abrahamsen, N. B. Christensen, F. Juranyi, N. H. Andersen, K. Lefmann, J. Andreasson, C. R. Bahl, and B. B. Iversen, *Nat. Mater.* **7**, 811 (2008).
- [37] Y. Xia, K. Pal, J. He, V. Ozoliņš, and C. Wolverton, *Phys. Rev. Lett.* **124**, 065901 (2020).
- [38] S. Mukhopadhyay, D. S. Parker, B. C. Sales, A. A. Puretzy, M. A. McGuire, and L. Lindsay, *Science* **360**, 1455

- (2018).
- [39] T. Björkman, V. Skakalova, S. Kurasch, U. Kaiser, J. C. Meyer, J. H. Smet, and A. V. Krashennnikov, [ACS Nano](#) **10**, 10929 (2016).
- [40] Z. Feng, Y. Fu, Y. Yan, Y. Zhang, and D. J. Singh, [Phys. Rev. B](#) **103**, 224101 (2021).
- [41] Y. Pang, J. Liu, X. Fan, H. Yang, J. Zhu, Z. Wang, Y. Yao, X. Qian, and R. Yang, [Phys. Rev. B](#) **108**, 205112 (2023).
- [42] Z. Tong, A. Pecchia, C. Yam, T. Dumitrica, and T. Frauenheim, [Nano Lett.](#) **23**, 9468 (2023).